

Article

Selected Class of Enamides Bearing Nitro Functionality as Dual-Acting with Highly Selective Monoamine Oxidase-B and BACE1 Inhibitors

Anusree Venkidath ^{1,†}, Jong Min Oh ^{2,†}, Sanal Dev ^{1,*}, Elham Amin ^{3,4}, Shebina P. Rasheed ¹, Ajeesh Vengamthodi ¹, Nicola Gambacorta ⁵, Ahmed Khames ⁶, Mohamed A. Abdelgawad ⁷, Ginson George ⁸, Orazio Nicolotti ⁵, Hoon Kim ^{2,*} and Bijo Mathew ^{8,*}

- ¹ Centre for Experimental Drug Design and Development, Department of Pharmaceutical Chemistry, Al-Shifa College of Pharmacy, Perinthalmanna 679325, India; anusreekousthubham96@gmail.com (A.V.); shebinaniz@gmail.com (S.P.R.); ajeeshvengan@hotmail.com (A.V.)
 - ² Department of Pharmacy, and Research Institute of Life Pharmaceutical Sciences, Suncheon National University, Suncheon 57922, Korea; 1205027@s.scnu.ac.kr
 - ³ Department of Medicinal Chemistry and Pharmacognosy, College of Pharmacy, Qassim University, Buraidah 52571, Saudi Arabia; elham_bns@yahoo.com
 - ⁴ Department of Pharmacognosy, Faculty of Pharmacy, Beni-Suef University, Beni-Suef 62514, Egypt
 - ⁵ Dipartimento di Farmacia-Scienze del Farmaco, Università Degli Studi di Bari "Aldo Moro", Via E. Orabona, 4, I-70125 Bari, Italy; nicola.gambacorta1@uniba.it (N.G.); orazio.nicolotti@uniba.it (O.N.)
 - ⁶ Department of Pharmaceutics and Industrial Pharmacy, College of Pharmacy, Taif University, P.O. Box 11099, Taif 21944, Saudi Arabia; a.khamies@tu.edu.sa
 - ⁷ Department of Pharmaceutical Chemistry, College of Pharmacy, Jouf University, Sakaka 72341, Saudi Arabia; mhmdgwd@ju.edu.sa
 - ⁸ Department of Pharmaceutical Chemistry, Amrita School of Pharmacy, Amrita Vishwa Vidyapeetham, AIMS Health Sciences Campus, Kochi 682041, India; ginsongeorge239@gmail.com
- * Correspondence: sanaldev@gmail.com (S.D.); hoon@sunchon.ac.kr (H.K.); bijovilaventgu@gmail.com or bijomathew@aims.amrita.edu (B.M.)
- † These authors contributed equally to this work.



Citation: Venkidath, A.; Oh, J.M.; Dev, S.; Amin, E.; Rasheed, S.P.; Vengamthodi, A.; Gambacorta, N.; Khames, A.; Abdelgawad, M.A.; George, G.; et al. Selected Class of Enamides Bearing Nitro Functionality as Dual-Acting with Highly Selective Monoamine Oxidase-B and BACE1 Inhibitors. *Molecules* **2021**, *26*, 6004. <https://doi.org/10.3390/molecules26196004>

Academic Editors: Andrea Trabocchi and Brullo Chiara

Received: 6 July 2021

Accepted: 20 September 2021

Published: 3 October 2021

Publisher's Note: MDPI stays neutral with regard to jurisdictional claims in published maps and institutional affiliations.



Copyright: © 2021 by the authors. Licensee MDPI, Basel, Switzerland. This article is an open access article distributed under the terms and conditions of the Creative Commons Attribution (CC BY) license (<https://creativecommons.org/licenses/by/4.0/>).

Abstract: A small series of nitro group-bearing enamides was designed, synthesized (NEA1–NEA5), and evaluated for their inhibitory profiles of monoamine oxidases (MAOs) and β -site amyloid precursor protein cleaving enzyme 1 (β -secretase, BACE1). Compounds NEA3 and NEA1 exhibited a more potent MAO-B inhibition (IC_{50} value = 0.0092 and 0.016 μ M, respectively) than the standards (IC_{50} value = 0.11 and 0.14 μ M, respectively, for lazabemide and pargyline). Moreover, NEA3 and NEA1 showed greater selectivity index (SI) values toward MAO-B over MAO-A (SI of >1652.2 and >2500.0, respectively). The inhibition and kinetics studies suggested that NEA3 and NEA1 are reversible and competitive inhibitors with K_i values of 0.013 ± 0.005 and 0.0049 ± 0.0002 μ M, respectively, for MAO-B. In addition, both NEA3 and NEA1 showed efficient BACE1 inhibitions with IC_{50} values of 8.02 ± 0.13 and 8.21 ± 0.03 μ M better than the standard quercetin value (13.40 ± 0.04 μ M). The parallel artificial membrane permeability assay (PAMPA) method demonstrated that all the synthesized derivatives can cross the blood–brain barrier (BBB) successfully. Docking analyses were performed by employing an induced-fit docking approach in the GLIDE module of Schrodinger, and the results were in agreement with their in vitro inhibitory activities. The present study resulted in the discovery of potent dual inhibitors toward MAO-B and BACE1, and these lead compounds can be fruitfully explored for the generation of newer, clinically active agents for the treatment of neurodegenerative disorders.

Keywords: monoamine oxidase; β -secretase; nitro group-bearing enamides; potent reversible inhibitor; dual-acting inhibitor; molecular docking

1. Introduction

The development of a new class of molecules for the complex pathology of neurodegenerative disorders, like Alzheimer's disease (AD) and Parkinson's disease (PD), is one of the most complicated zones in medicinal chemistry [1]. Multi-target-directed ligands (MTDLs) have led to a new paradigm that has emerged in recent times, in which the newly designed molecular scaffold is able to bind to different types of biologic targets that are interconnected with similar biochemical pathways [2,3]. The MTDLs design strategy includes the combination of two pharmacologically active molecules into a single framework, or keeping the most active functional moieties of different molecules in a single hybrid molecule [4].

The oxidative deamination of monoamine-related neurotransmitters and their regulation in the central and peripheral systems are controlled by flavin-dependent monoamine oxidases (MAOs) isoenzymes, such as MAO-A and MAO-B [5,6]. Selective inhibitions by MAO-B inhibitors are considered to be a promising neuronal pharmacotherapy for AD and PD [7]. The oxidative stress provoked by the metabolism of MAO-B leads to the cognitive destruction and aggregation of neurofibrillary tangles in PD patients [8,9]. Recently, many scaffolds, like chalcones, coumarins, chromones, pyrazolines, quinazolines, isatins, and thiazolidinones, which are derivatives of FDA approved MAO-B inhibitors, showed selective, reversible, and competitive types of MAO-B inhibition [10–18].

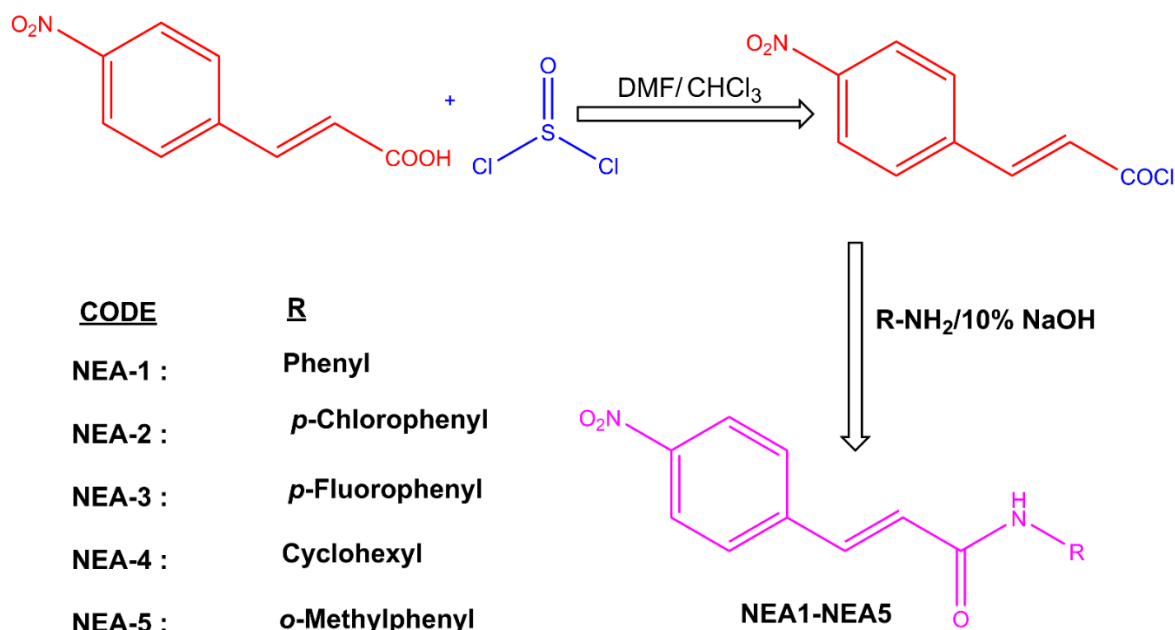
The presence of α,β -unsaturated ketone, carboxamide, multi-conjugated ketone, and olefinic linkage contribute to the versatility of the pharmacophore features of selective MAO-B inhibitors [19–24]. Recently, our group developed a new class of enamide-based MAO-B inhibitors by combining an olefinic linkage to the amide functional group. The resulting enamide linker with nitrophenyl hydrophobic candidate showed potent and selective MAO-B inhibition. The study documented that the presence of an electron-withdrawing nitro group has better binding affinity than electron-donating groups. Compound N-(3-nitrophenyl)prop-2 enamide (**AD9**) was an effective competitive inhibitor of MAO-B with K_i value of $0.039 \pm 0.005 \mu\text{M}$ [25]. In addition, numerous reports suggested that nitro groups are versatile electron-attracting functional groups, which are used in many of the FDA-approved drugs. This unique functional group can act as a proton acceptor, which can contribute to hydrogen-bonding interactions within the catalytic site of a variety of enzyme targets [26,27]. Prompted by this observation, we expanded our examination of structure activity relationships (SARs) of enamide-based MAO-B inhibitors by keeping nitrophenyl functionalities with other selected classes of enamide-based compounds.

The inhibition of the β -site amyloid precursor protein-cleaving enzyme-1 (BACE1) is one of the other attractive objectives when treating AD [28]. BACE1 inhibitors that are currently in different stages of clinical trials, such as Verubecestat, Elenbecestat, and Atabecestat, have an amide functional moiety as the crucial pharmacophore feature [29]. In this research, we focused our attention on the development of a small library of nitro-substituted enamide derivatives with dual-acting MAO-B and BACE1 inhibitors. The design and development of MTDLs has become authoritative in the selection of the starting scaffolds to develop a multifunctional molecular framework. The objective of the work is the synthesis and characterization of a selected class of nitro-bearing enamides. All the molecules were further subjected to enzyme inhibition studies against MAO-A, MAO-B, and BACE1. The topmost active compounds were exploited for their kinetics, reversibility properties, parallel artificial membrane permeability assay (PAMPA), and docking analyses.

2. Results and Discussion

2.1. Chemistry

The selected class of compound was synthesized by the following approach (Scheme 1). The spectral data are provided in the Supplementary Materials. The structures of the compounds were verified with reference to previously published literature [30,31].



Scheme 1. Synthesis of enamides.

2.2. Studies of MAOs and BACE1 Inhibitors

All of the screened compounds effectively inhibited MAO-B with residual activities of <50% at 10 μ M. However, these compounds showed a greater residual activity toward MAO-A (>83.5% at 10 μ M, except **NEA-3**) over MAO-B, indicating that these compounds possess greater inhibitory potential for MAO-B (Table 1). Compounds **NEA3** and **NEA1** exhibited the most potential activity toward MAO-B (IC_{50} value = 0.0092 and 0.016 μ M, respectively) (Table 1). Unsubstituted enamide (**NEA1**) exerted an IC_{50} of 0.016 μ M. Substitution of numerous functionalities exerted a varied MAO-B inhibitory profile. For instance, a strong electron-withdrawing group (-F atom) at the *para* position resulted in the formation of a more potent component (**NEA3**; IC_{50} = 0.0092 μ M) than the parent (**NEA3**). Interestingly, an electron-donating substituent (**NEA5** with methyl functionalities at the *ortho* side) also resulted in the enhancement of MAO-B inhibition. It is noteworthy that the -Cl atom on the *para* position in **NEA2** resulted in the weakening of MAO-B inhibitory activity. This needs to be investigated further. In these derivatives, MAO-B inhibitory activities increased with the presence of *para*-F (**NEA3**) > -H (**NEA1**) > *ortho*-CH₃ (**NEA5**) > *para*-Cl (**NEA2**) (Table 1). The selectivity for MAO-B over MAO-A was also observed in terms of the selectivity index (SI), where **NEA1** and **NEA3** exerted high SI values of 2500 and 1652.2, respectively (Table 1). In addition, as represented in Table 1, **NEA1**, **NEA3**, and **NEA5** exerted great inhibitory potentials toward BACE1 (IC_{50} = 8.21, 8.02, and 17.7 μ M, respectively). The IC_{50} values of **NEA1** and **NEA3** were lower than the reference quercetin (IC_{50} = 13.4 μ M). Quercetin has been used as a reference for BACE1 inhibition, and the IC_{50} values ranged between 8.65 and 20.18 μ M [32–34]. On the other hand, all of the compounds weakly inhibited acetylcholinesterase and butyrylcholinesterase, with the residual activities of >76.5% at 10 μ M.

Recently, our group developed some trimethoxy halogenated chalcones as dual-acting MAO-B and BACE1 inhibitors that exhibited activities in the range of 0.84 to 4.17 μ M and 13.6 to 19.8 μ M, respectively [35]. In another study, phytochemicals from *Rauwolfia serpentina* roots were evaluated for their MTDL efficiencies, while indole alkaloids (reserpine and ajmalicine) were evaluated as potential agents for MAO-B and BACE1 inhibition with dose-dependent activities [36]. It is noteworthy that the replacement of chalcones with enamides resulted in the enhancement of overall MAO-B and BACE1 inhibitory activities.

Interestingly, the analogues which we tested resulted in potent inhibitory activities in nanomolar ranges towards MAO-B inhibition.

Table 1. MAOs and BACE1 inhibition profiles of nitro-bearing enamides ^a.

Compounds	% Residual Activity (at 10 μ M)			IC ₅₀ (μ M)			SI ^b
	MAO-A	MAO-B	BACE1	MAO-A	MAO-B	BACE1	
NEA1	91.9 \pm 5.9	3.88 \pm 0.6	34.9 \pm 0.5	>40	0.016 \pm 0.001	8.21 \pm 0.03	>2500.0
NEA2	95.0 \pm 0.5	35.8 \pm 6.2	88.1 \pm 0.3	>40	5.28 \pm 0.09	-	>7.58
NEA3	61.9 \pm 0.4	3.04 \pm 0.5	34.4 \pm 0.2	15.2 \pm 0.6	0.0092 \pm 0.0003	8.02 \pm 0.13	>1652.2
NEA4	85.6 \pm 1.7	9.52 \pm 3.5	61.2 \pm 3.0	>40	0.074 \pm 0.020	-	>540.5
NEA5	83.5 \pm 1.3	8.67 \pm 2.3	44.0 \pm 0.2	>40	0.038 \pm 0.003	17.70 \pm 1.70	>1052.6
Toloxatone	-	-	-	1.08 \pm 0.03	-	-	-
Lazabemide	-	-	-	-	0.11 \pm 0.02	-	-
Clorgyline	-	-	-	0.007 \pm 0.001	-	-	-
Pargyline	-	-	-	-	0.14 \pm 0.01	-	-
Quercetin	-	-	-	-	-	13.40 \pm 0.04	-

^a Results are the means \pm S.E.M. of duplicate or triplicate experiments. ^b Selectivity index (SI) values are expressed for MAO-B as compared with MAO-A.

2.3. Kinetics

The most potent compounds, **NEA1** and **NEA3**, were further subjected to enzyme-inhibition kinetics. The obtained results are represented in Figure 1. As represented in Lineweaver–Burk plots, all of the lines converged at the y-intercept ($1/V_{max}$), suggesting the scope of the competitive mode of inhibition by these compounds. The K_i values were deduced from the secondary plot, and were found to be 0.013 ± 0.005 and 0.0049 ± 0.0002 μ M for **NEA1** and **NEA3**, respectively. These results suggest the competitive mode of inhibition by these compounds at the active site of MAO-B.

2.4. Reversibility Studies

The reversibility patterns of the potent compounds were analyzed by comparing the relative activities in undialyzed (A_U) and dialyzed (A_D) samples at the following concentrations: **NEA1** = 0.032 μ M; **NEA3** = 0.020 μ M; lazabemide = 0.22 μ M; and pargyline = 0.28 μ M. Lazabemide is a reversible inhibitor of MAO-B, while pargyline is an irreversible inhibitor of MAO-B; thus, they were selected as reference standards. In the case of **NEA1**, the MAO-B inhibition was recovered from 29.2% (A_U) to 79.5% (A_D), while for **NEA3** it went from 32.8% to 79.5% (Figure 2). These recovery values were similar to the reversible reference inhibitor (lazabemide), which went from 29.7% to 82.8%, and could be distinguished to pargyline, an irreversible reference inhibitor, which went from 26.6% to 28.7%. These results indicate that **NEA1** and **NEA3** function as reversible MAO-B inhibitors.

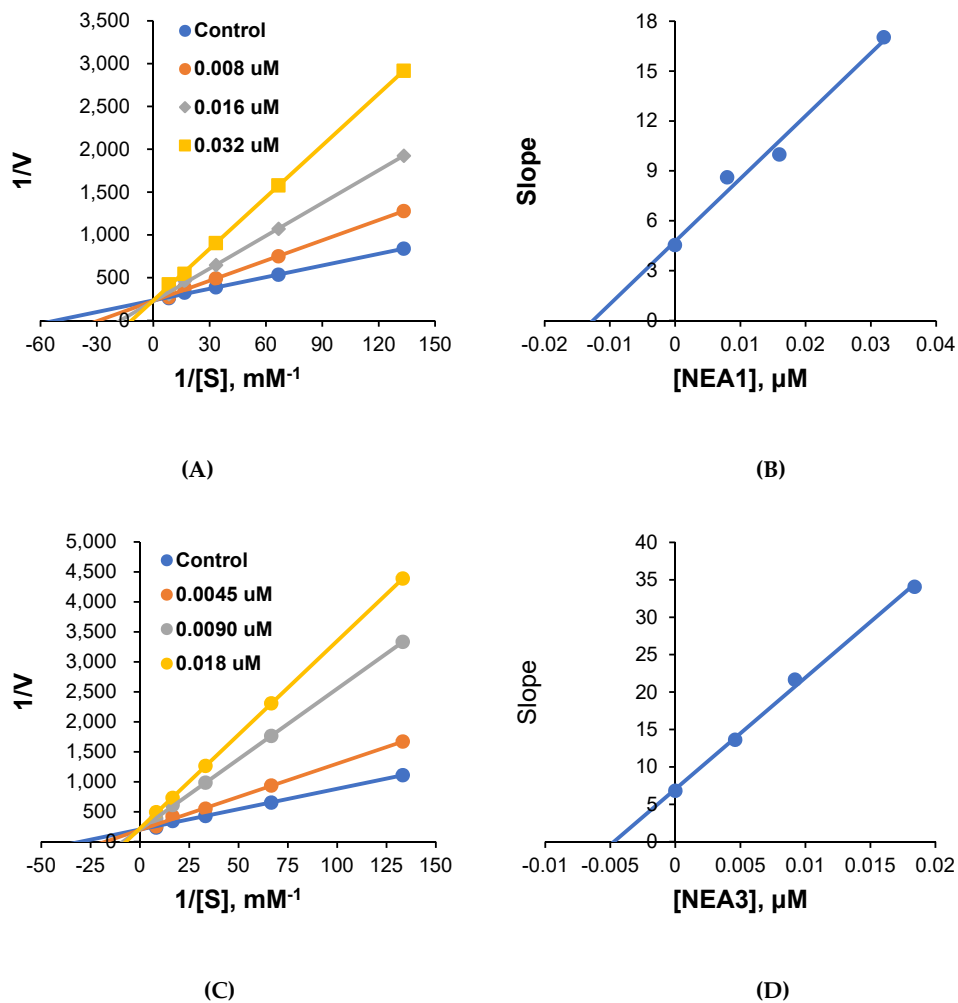


Figure 1. Lineweaver–Burk plots for MAO-B inhibition by NEA1 and NEA3 (A,C), and their respective secondary plots (B,D) of the slopes vs. inhibitor concentrations.

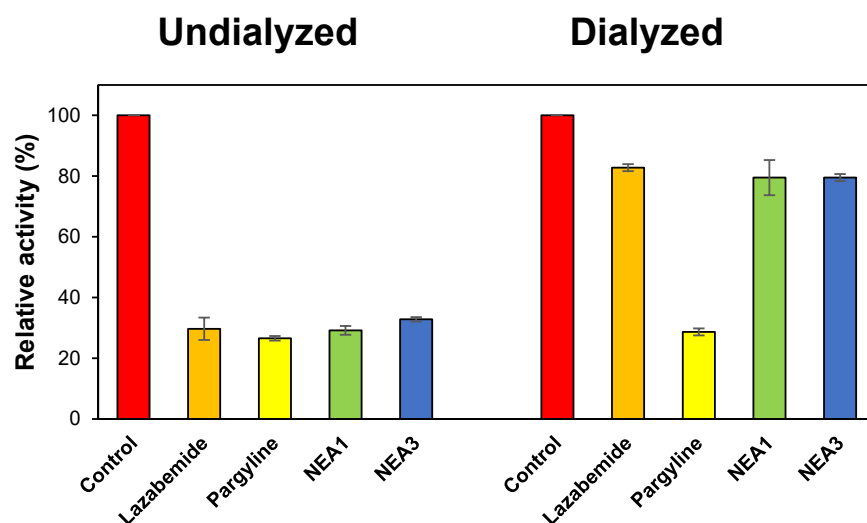


Figure 2. Recoveries of MAO-B inhibitions by NEA1 and NEA3 using dialysis experiments. Dialysis was performed for 6 h with a buffer change after 3 h with duplicate experiments.

2.5. Blood–Brain Barrier (BBB) Permeation Studies

The CNS bioavailability of the molecules was further ascertained by the PAMPA method [37]. Highly effective permeability and high CNS bioavailability were observed for all the enamides tested, with Pe ranges between 13.46×10^{-6} and 16.43×10^{-6} cm/s (Table 2).

Table 2. BBB assay of enamide derivatives (NEA1–NEA5) using the PAMPA method.

Compounds	Bibliography [34] Pe ($\times 10^{-6}$ cm/s)	Experimental Pe ($\times 10^{-6}$ cm/s)	Prediction
NEA1		14.44 ± 0.35	CNS+
NEA2		13.46 ± 0.26	CNS+
NEA3		16.43 ± 0.17	CNS+
NEA4		15.54 ± 0.62	CNS+
NEA5		15.53 ± 0.44	CNS+
Progesterone	9.3	9.12 ± 0.21	CNS+
Verapamil	16.0	16.33 ± 0.44	CNS+
Piroxicam	2.5	2.37 ± 0.33	CNS±
Lomefloxacin	1.1	1.31 ± 0.51	CNS–
Dopamine	0.2	0.26 ± 0.04	CNS–

CNS+ (high BBB permeation predicted: Pe (10^{-6} cm/s) > 4.00). CNS– (low BBB permeation predicted: Pe (10^{-6} cm/s) < 2.00). CNS± (BBB permeation uncertain: Pe (10^{-6} cm/s) from 2.00 to 4.00).

2.6. Computational Studies

In silico analyses were performed at the molecular level to deepen the interactions between compounds NEA1 and NEA3 and enzymes BACE1 and MAO-B. Figures 3 and 4 show the results of induced-fit docking.

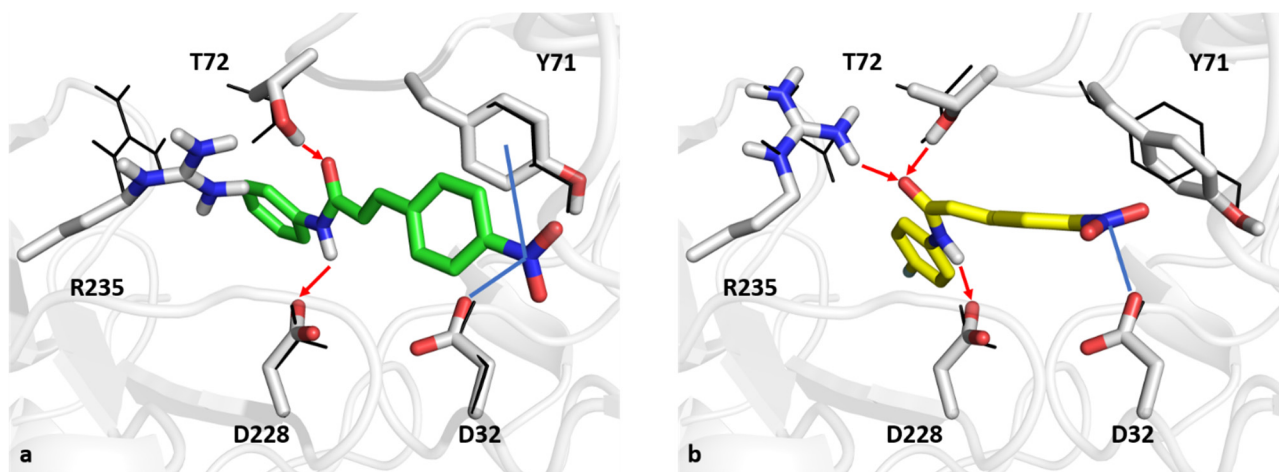


Figure 3. The best-docked poses of compounds NEA1 (a, green sticks) and NEA3 (b, yellow sticks) in a BACE1 binding pocket. Blue lines and red arrows indicate ion-dipole interactions and hydrogen bonds, respectively. Black wireframes report the original pose of BACE1 sidechains in the binding site.

As far as interactions within BACE1 are concerned, the NEA1 compound can make hydrogen bonds with T72 and the catalytic D228 with its enamide moiety. Moreover, the *para*-nitro substituent can make an ion-dipole interaction with the catalytic D32 and a dipole interaction with Y71 at S1. On the other hand, the enamide moiety of compound NEA3 can establish hydrogen bonds with the catalytic D228 and T72 as reported for NEA1 and, in addition, with R235. Furthermore, the *para*-nitro group can interact through ion-dipole interaction with catalytic D32. For the sake of completeness, docking scores for NEA1 and NEA3 were equal to 6.656 and 7.191 kcal/mol, respectively.

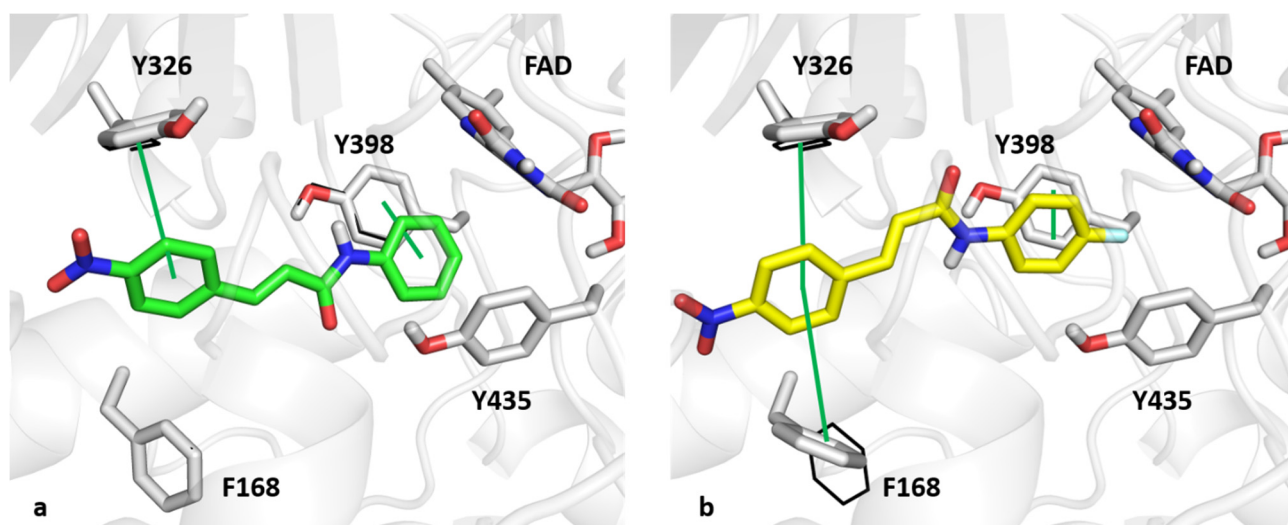


Figure 4. The best-docked poses of compounds **NEA1** (a, green sticks) and **NEA3** (b, yellow sticks) in a MAO-B binding pocket. Green lines indicate p–p contacts. Black wireframes report the original pose of MAO-B sidechains within the binding site.

As for the MAO-B binding pocket, **NEA1** and **NEA3** assumed a similar binding mode within the MAO-B active site. The *para*-nitro aromatic ring of **NEA1** was able to make p–p contact with the MAO-B selective residue, Y326, and the phenyl ring that resulted was placed in a network of hydrophobic interactions with FAD, Y435, and Y398, the latter also being involved in p–p contact. Regarding the binding mode of **NEA3**, the *para*-nitro aromatic ring that resulted was sandwiched between Y326 and F168. Furthermore, the *para*-fluorine ring was able to interact with Y398 through p–p contact, which resulted in it being trapped in the aromatic cage that Y398, Y435, and FAD formed. Docking score values obtained from simulations of **NEA1** and **NEA3** were found to be -9.977 and -10.453 kcal/mol, respectively.

Computational studies have shed light on the interaction between compounds **NEA1** and **NEA3** toward BACE1 and MAO-B. Interestingly, the induced-fit docking protocol can give a more accurate and detailed description of the binding modes of the two compounds. As far as BACE1 is concerned, the conformation of the two catalytic aspartate residues (D32 and D228) slightly changed for the optimal interaction with the two compounds. In addition, the carbonyl group of the enamides formed a hydrogen bond with the conformation T72 residue located in the FLAP region. Furthermore, R235 was particularly affected by the induced-fit docking, favoring the interaction with the enamide moiety of compound **NEA3**. As for MAO-B, the only residues involved in a change of its conformation state was F168, whose movement allowed the T-shape p–p contact with the *para*-nitro aromatic ring of compound **NEA3**.

3. Materials and Methods

3.1. Synthesis

The synthesis of the target molecules is depicted in Scheme 1. Initially, 4-nitrocinnamic acid (5 mmol, i.e., 1.0 g) was added into a 100 mL two-neck flask containing 20 mL of chloroform. Four drops of DMF were added slowly to the flask and stirred for 15 min at room temperature (RT). Thionyl chloride (10 mmol, 2 mL) was added and heated to reflux at 50–60 °C for 5 h. After completion of the reaction, the excess thionyl chloride was distilled off to obtain 4-nitrocinnamoyl chloride as a yellow solid. It was then transferred into a 250 mL flask containing a mixture of respective amines (10 mmol) and 50 mL of 10% NaOH. The reaction was stirred at RT until the completion of the reaction was confirmed by TLC. The final compounds were obtained by recrystallization from hot ethanol.

3.1.1. 3-(4-Nitrophenyl)-*N*-phenylacrylamide (NEA1)

Whitish-yellow powder; M.P. 210–212 °C; R_f value: 0.68 (*n*-hexane ethyl acetate = 2:0.5); IR (ZnSe): 3305 cm⁻¹ (N-H stretching in amide), 1655 cm⁻¹ (C=O stretching in amide), 1621 cm⁻¹ (Ar-CH=CHR), 1592 cm⁻¹ (Ar C-C stretching), 652 cm⁻¹ (=CH out of plane in trans RHC=CHR); ¹H NMR (500 MHz) DMSO-*d*₆ δ ppm: 10.35 (s, 1H, NH), 8.30 (d, *J* = 5, 1H, CH), 7.91–7.81 (m, 2H), 7.01–7.91 (m, 9H, Ar H); ¹³C NMR (125 MHz) DMSO-*d*₆: 119.28, 123.58, 124.09, 126.55, 128.66, 128.78, 137.61, 138.98, 141.25, 147.57, 162.75; ESI-MS (*m/z*): 269.0138 [M + 1].

3.1.2. *N*-(4-Chlorophenyl)-3-(4-nitrophenyl)acrylamide (NEA2)

Brownish-yellow powder; M.P. 224–226 °C; R_f value: 0.8 (*n*-hexane ethyl acetate = 2:0.5); IR (ZnSe): 3377 cm⁻¹ (N-H stretching in amide), 1608 cm⁻¹ (C=O stretching in amide), 815 cm⁻¹ (C-Cl stretching), 1490 cm⁻¹ (Ar C-C stretching), 692 cm⁻¹ (=CH out of plane in trans RHC=CHR); ¹H NMR (500 MHz) DMSO-*d*₆ δ ppm: 10.49 (s, 1H, NH), 8.29–8.30 (d, *J* = 5 2H, CH), 6.98–7.91 (m, 8H, Ar H); ¹³C NMR (125 MHz) DMSO-*d*₆: 24.48, 25.20, 32.36, 47.72, 124.09, 126.84, 128.50, 136.13, 141.65, 147.43, 163.27; ESI-MS (*m/z*): 301.1145 [M + 1].

3.1.3. *N*-(4-Fluorophenyl)-3-(4-nitrophenyl)acrylamide (NEA3)

Whitish-yellow powder; M.P. 208–210 °C; R_f value: 0.61 (*n*-hexane ethyl acetate = 2:0.5); IR (ZnSe): 3289 cm⁻¹ (N-H stretching in amide), 1606 cm⁻¹ (C=O stretching in amide), 1402 cm⁻¹ (Ar C-C stretching), 958 cm⁻¹ (C-F stretching), 706 cm⁻¹ (=CH out of plane in trans RHC=CHR); ¹H NMR (125 MHz) DMSO-*d*₆ δ ppm: 10.49 (s, 1H, NH), 8.30–8.28 (d, *J* = 10 2H, CH), 6.97–7.91 (m, 8H, Ar H); ¹³C NMR (125 MHz) DMSO-*d*₆: 115.39, 120.95, 124.01, 126.25, 128.61, 135.31, 137.61, 141.12, 147.51, 157.13, 159.04, 162.57; ESI-MS (*m/z*): 287.0211 [M + 1].

3.1.4. *N*-Cyclohexyl-3-(4-nitrophenyl)acrylamide (NEA4)

Whitish-yellow powder; M.P. 166–168 °C; R_f value: 0.49 (*n*-hexane ethyl acetate = 2:0.5); IR (ZnSe): 3370 cm⁻¹ (N-H stretching in amide), 2935 cm⁻¹ (C-H stretching), 1618 cm⁻¹ (C=O stretching in amide), 725 cm⁻¹ (=CH out of plane in trans RHC=CHR); ¹H NMR (500MHz) DMSO-*d*₆ δ ppm: 8.27–8.25 (d, *J* = 10, 2H, CH), 8.14 (1H, NH), 6.81–8.12 (m, 4H, Ar-H), 3.65–3.69 (m, 1H, cyclohexyl), 1.18–1.82 (m, 10H, cyclohexyl); ¹³C NMR (125 MHz) DMSO-*d*₆: 24.48, 25.20, 32.36, 47.72, 124.09, 126.84, 128.50, 136.13, 141.65, 147.43, 163.27; ESI-MS (*m/z*): 275.0888 [M + 1].

3.1.5. 3-(4-Nitrophenyl)-*N*-(*O*-tolyl)acrylamide (NEA5)

Whitish-yellow powder; M.P. 200–203 °C; R_f value: 0.58 (*n*-hexane ethyl acetate = 2:0.5); IR (ZnSe): 3270 cm⁻¹ (N-H stretching in amide), 1615 cm⁻¹ (C=O stretching in amide), 2918 cm⁻¹ (C-H stretching), 1450 cm⁻¹ (Ar C-C stretching), 720 cm⁻¹ (=CH out of plane in trans RHC=CHR); ¹H NMR (500 MHz) DMSO-*d*₆ δ ppm: 9.61 (s, 1H, NH), 8.30–8.29 (d, *J* = 10 2H, CH), 7.09–7.91 (m, 8H, Ar-H), 2.26 (s, 3H, -CH₃); ¹³C NMR (125 MHz) DMSO-*d*₆: 17.82, 124.05, 124.22, 125.10, 125.92, 126.52, 128.62, 130.28, 130.94, 136.05, 137.46, 141.33, 147.51, 162.82; ESI-MS (*m/z*): 283.0648 [M + 1].

3.2. Enzyme Inhibition Studies

MAO inhibitory assay was assessed in accordance with the previously standardized methods of assessing recombinant MAO-A and MAO-B by using the substrates (0.06 mM kynuramine and 0.3 mM benzylamine, respectively) [38–40]. Toloxatone/clorgyline and lazabemide/pargyline were used as reference standards for MAO-A and MAO-B, respectively. The K_m of benzylamine for MAO-B was 0.027 mM. The BACE1 activity was measured using a commercially available assay kit (β-secretase, CS0010). An excitation wavelength of 320 nm and an emission wavelength of 405 nm were used in a fluorescence spectrometer (FS-2, Scinco, Seoul, Korea) [41]. Quercetin was used as a reference compound

for BACE1. The enzymes and chemicals were purchased from Sigma-Aldrich (St. Louis, MO, USA).

3.3. Enzyme Inhibition and Kinetic Studies

Initially, the inhibitory activities of the synthesized compounds were identified at a concentration of 10 μM against MAO-A, MAO-B, and BACE1. Further, the IC_{50} of the compounds which had less than 50% of residual activity were identified for each of the respective enzymes. The obtained IC_{50} values thus compared were used to deduce the SI values. Five different concentrations of the substrates were used in the kinetic experiments. The enzyme kinetics and inhibition patterns were analyzed using the Lineweaver–Burk plots and their secondary plots, under three inhibitor concentrations [42].

3.4. Inhibitor-Reversibility Analysis

The reversibility of MAO-B inhibition by **NEA1** and **NEA3** was evaluated using a standardized dialysis method [26]. Initially, the enzyme was preincubated with the screened compounds for 30 min at $\sim 2 \times \text{IC}_{50}$ (i.e., 0.032 and 0.020 μM , respectively). Lazabemide (0.22 μM) and pargyline (0.28 μM) were used as reference standards for reversible and irreversible MAO-B inhibitors, respectively. The activities in dialyzed (A_D) and undialyzed (A_U) samples were compared and reversibility patterns were determined [43].

3.5. Computational Studies

Computational studies of compounds **NEA1** and **NEA3** were performed on X-ray structures of BACE1 (PDB ID: 3TPP) and MAO-B (PDB ID: 2V5Z), whose crystals were retrieved from the Protein Data Bank [44,45]. Geometrical optimization and energetic minimization steps were carried out on proteins by using the Protein Preparation Tools available on the Schrodinger Suite [46]. Ligands were prepared with the Ligprep Tool. The enclosing boxes were centered on cognate ligands [47]. The induced-fit protocol was used by employing GLIDE software with the OLPS3 force field, for the purpose of inspecting the binding mode of ligands as well as the conformational changes in the targets' sidechains, thus increasing the accuracy and reliability of the results with respect to the standard docking protocols, for which such structural changes are not detectable. Sidechain refinement was carried out on residues within 6 Å of ligand poses together with Glide SP redocking of each protein–ligand complex structure within 30.0 kcal/mol of the lowest energy [48–51].

4. Conclusions

A selected class of enamides bearing nitro pharmacophore was designed, synthesized, and evaluated for its dual inhibitory activities against MAO-A, MAO-B, and BACE1. Treatment of 4-nitrocinnamic acid with thionyl chloride resulted in the formation of acid chloride, and further reactions with selected substituted primary amines afforded the analogues (**NEA1** to **NEA5**). Among these compounds, **NEA3** and **NEA1** exerted more potent MAO-B activities ($\text{IC}_{50} = 0.0092$ and 0.016 μM , respectively) than the standard drugs (lazabemide and pargyline; $\text{IC}_{50} = 0.11$ and 0.14 μM , respectively). Moreover, these analogues exerted >1650-fold selectivity toward the MAO-B over MAO-A. A similar trend was observed in the case of BACE1 inhibition, wherein **NEA3** and **NEA1** exerted inhibitory activities with IC_{50} values of 8.01 and 8.21 μM , respectively. Enzyme kinetics of these analogues revealed a competitive and reversible inhibitory mode toward MAO-B. Molecular modeling studies further supported the ability of these analogues in their potential inhibitory activities. In summary, the present study identified the potent lead molecules, which will pave the way for new clinical agents for the treatment of neurodegenerative disorders.

Supplementary Materials: The following are available online. ^1H - and ^{13}C -NMR spectral data of the compounds are available in the Supplementary Materials.

Author Contributions: Conceptualization: A.V. (Anusree Venkidath), B.M., S.D. and H.K.; Biological activity: J.M.O.; Kinetics: J.M.O.; Docking analysis: N.G. and O.N.; Synthesis: A.V. (Anusree Venkidath), S.D., S.P.R., A.K., M.A.A. and A.V. (Ajeesh Vengamthodi); PAMPA assay: E.A.; Data curation: J.M.O., G.G. and B.M.; Writing—original draft preparation: J.M.O., N.G. and G.G.; Writing—review and editing: O.N., B.M. and H.K.; Supervision: H.K. All authors have read and agreed to the published version of the manuscript.

Funding: This research received no external funding.

Institutional Review Board Statement: Not applicable.

Informed Consent Statement: Not applicable.

Data Availability Statement: Not applicable.

Acknowledgments: Authors acknowledge Taif University Researchers Supporting Project number (TURSP-2020/68), Taif University, Taif, Saudi Arabia (A.K.), and the Deanship of Scientific Research, Qassim University, Buraidah, Saudi Arabia (E.A.).

Conflicts of Interest: The authors declare no conflict of interest.

Sample Availability: Samples of the compounds used in this study are available from the authors.

References

1. Morphy, R.; Rankovic, Z. Designed multiple ligands. An emerging drug discovery paradigm. *J. Med. Chem.* **2005**, *48*, 6523–6543. [[CrossRef](#)]
2. Geldenhuys, W.J.; Youdim, M.B.H.; Carroll, R.T.; Van der Schyf, C.J. The emergence of designed multiple ligands for neurodegenerative disorders. *Prog. Neurobiol.* **2011**, *94*, 347–359. [[CrossRef](#)]
3. Morphy, R.; Kay, C.; Rankovic, Z. From magic bullets to designed multiple ligands. *Drug Discov. Today* **2004**, *9*, 641–651. [[CrossRef](#)]
4. Rodríguez-Soacha, D.A.; Scheiner, M.; Decker, M. Multi-target-directed-ligands acting as enzyme inhibitors and receptor ligands. *Eur. J. Med. Chem.* **2019**, *180*, 690–706. [[CrossRef](#)] [[PubMed](#)]
5. Kumar, B.; Gupta, V.P.; Kumar, V.A. Perspective on monoamine oxidase enzyme as drug target: Challenges and opportunities. *Curr. Drug Targets* **2017**, *18*, 87–97. [[CrossRef](#)] [[PubMed](#)]
6. Mathew, B.; Mathew, G.E.; Suresh, J.; Ucar, G.; Sasidharan, R.; Anbazhagan, S.; Vilapurathu, J.K.; Jayaprakash, V. Monoamine oxidase inhibitors: Perspective design for the treatment of depression and neurological disorders. *Curr. Enzyme Inhib.* **2016**, *12*, 115–122. [[CrossRef](#)]
7. Tripathi, A.C.; Upadhyay, S.; Paliwal, S.; Saraf, S.K. Privileged scaffolds as MAO inhibitors: Retrospect and prospects. *Eur. J. Med. Chem.* **2018**, *145*, 445–497. [[CrossRef](#)] [[PubMed](#)]
8. Manzoor, S.; Hoda, N.A. Comprehensive review of monoamine oxidase inhibitors as anti-Alzheimer's disease agents: A review. *Eur. J. Med. Chem.* **2020**, *206*, 112787. [[CrossRef](#)] [[PubMed](#)]
9. Tripathi, R.K.P.; Ayyannan, S.R. Monoamine oxidase-B inhibitors as potential neurotherapeutic agents: An overview and update. *Med. Res. Rev.* **2019**, *39*, 1603–1706. [[CrossRef](#)] [[PubMed](#)]
10. Guglielmi, P.; Mathew, B.; Secci, D.; Carradori, S. Chalcones: Unearthing their therapeutic possibility as monoamine oxidase B inhibitors. *Eur. J. Med. Chem.* **2020**, *205*, 112650. [[CrossRef](#)] [[PubMed](#)]
11. Koyiparambath, V.P.; Prayaga Rajappan, K.; Rangarajan, T.M.; Al-Sehemi, A.G.; Pannipara, M.; Bhaskar, V.; Nair, A.S.; Sudevan, S.T.; Kumar, S.; Mathew, B. Deciphering the detailed structure-activity relationship of coumarins as Monoamine oxidase enzyme inhibitors-An updated review. *Chem. Biol. Drug Des.* **2021**. [[CrossRef](#)]
12. Patil, P.O.; Bari, S.B.; Firke, S.D.; Deshmukh, P.K.; Donda, S.T.; Patil, D.A. A comprehensive review on synthesis and designing aspects of coumarin derivatives as monoamine oxidase inhibitors for depression and Alzheimer's disease. *Bioorg. Med. Chem.* **2013**, *21*, 2434–2450. [[CrossRef](#)]
13. Mathew, B.; Mathew, G.E.; Petzer, J.P.; Petzer, A. Structural exploration of synthetic chromones as selective MAO-B inhibitors: A Mini Review. *Comb. Chem. High Throughput Screen.* **2017**, *20*, 522–532. [[CrossRef](#)]
14. Secci, D.; Carradori, S.; Bolasco, A.; Bizzarri, B.; D'Ascenzio, M.; Maccioni, E. Discovery and optimization of pyrazoline derivatives as promising monoamine oxidase inhibitors. *Curr. Top. Med. Chem.* **2012**, *12*, 2240–2257. [[CrossRef](#)]
15. Rehuman, N.A.; Al-Sehemi, A.G.; Parambi, D.G.T.; Rangarajan, T.M.; Nicolotti, O.; Kim, H.; Mathew, B. Current progress in quinazoline derivatives as acetylcholinesterase and monoamine oxidase inhibitors. *ChemistrySelect* **2021**, *6*, 7162. [[CrossRef](#)]
16. Helguera, A.M.; Perez-Machado, G.; Cordeiro, M.N.; Borges, F. Discovery of MAO-B inhibitors—Present status and future directions part I: Oxygen heterocycles and analogs. *Mini Rev. Med. Chem.* **2012**, *12*, 907–919. [[CrossRef](#)] [[PubMed](#)]
17. Carradori, S.; Silvestri, R. New frontiers in selective human MAO-B inhibitors. *J. Med. Chem.* **2015**, *58*, 6717–6732. [[CrossRef](#)] [[PubMed](#)]
18. Mathew, B. Privileged pharmacophore of FDA approved drugs in combination with chalcone framework: A new hope for Alzheimer's treatment. *Comb. Chem. High Throughput Screen.* **2020**, *23*, 842–846. [[CrossRef](#)]

19. Mellado, M.; González, C.; Mella, J.; Aguilar, L.F.; Viña, D.; Uriarte, E.; Cuellar, M.; Matos, M.J. Combined 3D-QSAR and docking analysis for the design and synthesis of chalcones as potent and selective monoamine oxidase B inhibitors. *Bioorg. Chem.* **2021**, *108*, 104689. [[CrossRef](#)]
20. Rodríguez-Enríquez, F.; Viña, D.; Uriarte, E.; Laguna, R.; Matos, M.J. 7-Amidocoumarins as multitarget agents against neurodegenerative diseases: Substitution pattern modulation. *Chem. Med. Chem.* **2021**, *16*, 179–186. [[CrossRef](#)]
21. Sellitepe, H.E.; Oh, J.M.; Doğan, İ.S.; Yildirim, S.; Aksel, A.B.; Jeong, G.S.; Khames, A.; Abdelgawad, M.A.; Gambacorta, N.; Nicolotti, O.; et al. Synthesis of *N'*-(4-/3-/2-/Non-substituted benzylidene)-4-[(4-methylphenyl)sulfonyloxy] benzohydrazides and evaluation of their inhibitory activities against monoamine oxidases and β -secretase. *Appl. Sci.* **2021**, *11*, 5830. [[CrossRef](#)]
22. Legoabe, L.; Kruger, J.; Petzer, A.; Bergh, J.J.; Petzer, J.P. Monoamine oxidase inhibition by selected anilide derivatives. *Eur. J. Med. Chem.* **2011**, *46*, 5162–5174. [[CrossRef](#)] [[PubMed](#)]
23. Maliyakkal, N.; Eom, B.H.; Heo, J.H.; Abdullah Almoyad, M.A.; Parambi, D.G.T.; Gambacorta, N.; Nicolotti, O.; Beeran, A.A.; Kim, H.; Mathew, B. A new potent and selective monoamine oxidase-B inhibitor with extended conjugation in a chalcone framework: 1-[4-(Morpholin-4-yl)phenyl]-5-phenylpenta-2,4-dien-1-one. *Chem. Med. Chem.* **2020**, *15*, 1629–1633. [[CrossRef](#)] [[PubMed](#)]
24. Carradori, S.; Secci, D.; Petzer, J.P. MAO inhibitors and their wider applications: A patent review. *Expert Opin. Ther. Pat.* **2018**, *28*, 211–226. [[CrossRef](#)]
25. Kavully, F.S.; Oh, J.M.; Dev, S.; Kaipakasseri, S.; Palakkathondi, A.; Vengamthodi, A.; Azeez, R.F.; Tondo, A.R.; Nicolotti, O.; Kim, H.; et al. Design of enamides as new selective monoamine oxidase-B inhibitors. *J. Pharm. Pharmacol.* **2020**, *72*, 916–926. [[CrossRef](#)]
26. Olender, D.; Żwawiak, J.; Zaprutko, L. Multidirectional efficacy of biologically active nitro compounds included in medicines. *Pharmaceuticals* **2018**, *11*, 54. [[CrossRef](#)]
27. Nepali, K.; Lee, H.Y.; Liou, J.P. Nitro-group-containing drugs. *J. Med. Chem.* **2019**, *62*, 2851–2893. [[CrossRef](#)]
28. Ghosh, A.K.; Osswald, H.L. BACE1 (β -secretase) inhibitors for the treatment of Alzheimer's disease. *Chem. Soc. Rev.* **2014**, *43*, 6765–6813. [[CrossRef](#)] [[PubMed](#)]
29. Moussa-Pacha, N.M.; Abdin, S.M.; Omar, H.A.; Alniss, H.; Al-Tel, T.H. BACE1 inhibitors: Current status and future directions in treating Alzheimer's disease. *Med. Res. Rev.* **2020**, *40*, 339–384. [[CrossRef](#)] [[PubMed](#)]
30. Pardin, C.; Keillor, J.W.; Lubell, W.D. Cinnamoyl Inhibitors of Transglutaminase. U.S. Patent 9,162,991, 20 November 2015.
31. Schultz, H.W.; Wiese, G.A. The synthesis of some derivatives of cinnamic acid and their antifungal action. *J. Am. Pharm. Assoc.* **1959**, *48*, 750–752. [[CrossRef](#)]
32. Park, J.H.; Whang, W.K. Bioassay-guided isolation of anti-Alzheimer active components from the aerial parts of *Hedyotis diffusa* and simultaneous analysis for marker compounds. *Molecules* **2020**, *25*, 5867. [[CrossRef](#)] [[PubMed](#)]
33. Youn, K.; Yoon, J.H.; Lee, N.; Lim, G.; Lee, J.; Sang, S.; Ho, C.T.; Jun, M. Nutrients. Discovery of sulforaphane as a potent BACE1 inhibitor based on kinetics and computational studies. *Nutrients* **2020**, *12*, 3026. [[CrossRef](#)] [[PubMed](#)]
34. Wagle, A.; Seong, S.H.; Zhao, B.T.; Woo, M.H.; Jung, H.A.; Choi, J.S. Comparative study of selective in vitro and in silico BACE1 inhibitory potential of glycyrrhizin together with its metabolites, 18 α - and 18 β -glycyrrhetic acid, isolated from *Hizikia fusiformis*. *Arch. Pharm. Res.* **2018**, *41*, 409–418. [[CrossRef](#)]
35. Vishal, P.K.; Oh, J.M.; Khames, A.; Abdelgawad, M.A.; Nair, A.S.; Nath, L.R.; Gambacorta, N.; Ciriaco, F.; Nicolotti, O.; Kim, H.; et al. Trimethoxylated halogenated chalcones as dual inhibitors of MAO-B and BACE1 for the treatment of neurodegenerative disorders. *Pharmaceutics* **2021**, *13*, 850. [[CrossRef](#)] [[PubMed](#)]
36. Kashyap, P.; Kalaiselvan, V.; Kumar, R.; Kumar, S. Ajmalicine and reserpine: Indole alkaloids as multi-target directed ligands towards factors implicated in Alzheimer's disease. *Molecules* **2020**, *25*, 1609. [[CrossRef](#)]
37. Di, L.; Kerns, E.H.; Fan, K.; McConnell, O.J.; Carter, G.T. High throughput artificial membrane permeability assay for blood-brain barrier. *Eur. J. Med. Chem.* **2003**, *38*, 223–232. [[CrossRef](#)]
38. Mathew, B.; Baek, S.C.; Grace Thomas Parambi, D.; Lee, J.P.; Joy, M.; Annie Rilda, P.R.; Randev, R.V.; Nithyamol, P.; Vijayan, V.; Inasu, S.T.; et al. Selected aryl thiosemicarbazones as a new class of multi-targeted monoamine oxidase inhibitors. *Med. Chem. Comm.* **2018**, *9*, 1871–1881. [[CrossRef](#)]
39. Lee, J.P.; Kang, M.G.; Lee, J.Y.; Oh, J.M.; Baek, S.C.; Leem, H.H.; Park, D.; Cho, M.L.; Kim, H. Potent inhibition of acetylcholinesterase by sargachromanol I from *Sargassum siliquastrum* and by selected natural compounds. *Bioorg. Chem.* **2019**, *89*, 103043. [[CrossRef](#)]
40. Heo, J.H.; Eom, B.H.; Ryu, H.W.; Kang, M.G.; Park, J.E.; Kim, D.Y.; Kim, J.H.; Park, D.; Oh, S.R.; Kim, H. Acetylcholinesterase and butyrylcholinesterase inhibitory activities of khellactone coumarin derivatives isolated from *Peucedanum japonicum* Thurnberg. *Sci Rep.* **2020**, *10*, 21695. [[CrossRef](#)]
41. Jeong, G.S.; Kang, M.G.; Han, S.A.; Noh, J.I.; Park, J.E.; Nam, S.J.; Park, D.; Yee, S.T.; Kim, H. Selective inhibition of human monoamine oxidase B by 5-hydroxy-2-methyl-chroman-4-one isolated from an endogenous lichen fungus *Daldinia fissa*. *J. Fungi* **2021**, *7*, 84. [[CrossRef](#)]
42. Mathew, B.; Oh, J.M.; Baty, R.S.; Batiha, G.E.; Parambi, D.G.T.; Gambacorta, N.; Nicolotti, O.; Kim, H. Piperazine-substituted chalcones: A new class of MAO-B, AChE, and BACE1 inhibitors for the treatment of neurological disorders. *Environ. Sci. Pollut. Res.* **2021**, *28*, 38855–38866. [[CrossRef](#)]

43. Nair, A.S.; Oh, J.-M.; Koyiparambath, V.P.; Kumar, S.; Sudevan, S.T.; Soremekun, O.; Soliman, M.E.; Khames, A.; Abdelgawad, M.A.; Pappachen, L.K.; et al. Development of halogenated pyrazolines as selective monoamine oxidase-B Inhibitors: Deciphering via molecular dynamics approach. *Molecules* **2021**, *26*, 3264. [[CrossRef](#)]
44. Xu, Y.; Li, M.; Greenblatt, H.; Chen, W.; Paz, A.; Dym, O.; Peleg, Y.; Chen, T.; Shen, X.; He, J.; et al. Flexibility of the flap in the active site of BACE1 as revealed by crystal structures and molecular dynamics simulations. *Acta Crystallogr. Sect. D Biol. Crystallogr.* **2012**, *68*, 13–25. [[CrossRef](#)] [[PubMed](#)]
45. Binda, C.; Wang, J.; Pisani, L.; Caccia, C.; Carotti, A.; Salvati, P.; Edmondson, D.E.; Mattevi, A. Structures of human monoamine oxidase B complexes with selective noncovalent inhibitors: Safinamide and coumarin analogs. *J. Med. Chem.* **2007**, *50*, 5848–5852. [[CrossRef](#)] [[PubMed](#)]
46. *Schrödinger Release 2020-4: Protein Preparation Wizard*; Prime, Schrödinger, LLC.: New York, NY, USA, 2020.
47. Sastry, G.M.; Adzhigirey, M.; Day, T.; Annabhimoju, R.; Sherman, W. Protein and ligand preparation: Parameters, protocols, and influence on virtual screening enrichments. *J. Comput. Aided Mol. Des.* **2013**, *27*, 221–234. [[CrossRef](#)] [[PubMed](#)]
48. *Schrödinger Release 2020-4: LigPrep*; Schrödinger, LLC.: New York, NY, USA, 2020.
49. Sherman, W.; Day, T.; Jacobson, M.P.; Friesner, R.A.; Farid, R. Novel procedure for modeling ligand/receptor induced fit effects. *J. Med. Chem.* **2006**, *49*, 534–553. [[CrossRef](#)]
50. Friesner, R.A.; Banks, J.L.; Murphy, R.B.; Halgren, T.A.; Klicic, J.J.; Mainz, D.T.; Repasky, M.P.; Knoll, E.H.; Shelley, M.; Perry, J.K.; et al. Glide: A new approach for rapid, accurate docking and scoring. 1. Method and assessment of docking accuracy. *J. Med. Chem.* **2004**, *47*, 1739–1749. [[CrossRef](#)]
51. Harder, E.; Damm, W.; Maple, J.; Wu, C.; Reboul, M.; Xiang, J.Y.; Wang, L.; Lupyan, D.; Dahlgren, M.K.; Knight, J.L.; et al. OPLS3: A force field providing broad coverage of drug-like small molecules and proteins. *J. Chem. Theory Comput.* **2016**, *12*, 281–296. [[CrossRef](#)]